Numerical Solution of the Continuous Waveguide Transition Problem

WILLIAM A. HUTING, MEMBER, IEEE, AND KEVIN J. WEBB, MEMBER, IEEE

Abstract—**Waveguide transitions are an essential part of many microwave systems. A simple transition between two sizes of rectangular waveguide is analyzed by using the generalized telegraphist's equation. Solutions are obtained using a new moment method technique, a Runge–Kutta algorithm, and an iterative numerical integration technique. The results are compared to previously published experimental and numerical data.**

I. INTRODUCTION

THE TE_{01} CIRCULAR waveguide mode is characterized by an attenuation which decreases monotonically with frequency [1]. Thus, operating in this mode at a frequency well above cutoff is a widely used method of achieving low-loss transmission over long distances (see, for example, [2]). This implies operation in the multimode regime. Unfortunately, many microwave power sources are not compatible with circular overmoded waveguide but instead with standard sizes of rectangular and circular waveguide. The problem of designing a transition between rectangular single-mode waveguide and circular overmoded waveguide has been studied by various researchers [3]–[8]. Another area of interest has been the task of designing a transition between two sizes of circular waveguide (e.g., [9] and [10]). However, only a relatively small number of papers have considered numerical approaches to the waveguide transition design problem [6], [7], [10]. These approaches can be divided into two classes: the solution of a system of ordinary differential equations [6], [7], [10], and an approximation of the transition as a series of steps and the subsequent use of a mode-matching technique [10]. A new approach to the differential equation method using the method of moments [11] is presented here. As a test problem, this technique is applied to a simple transition between two sizes of rectangular waveguide, as illustrated in Fig. 1. Other approaches are also discussed. The results obtained here are compared to previously published experimental [12] and numerical [7] data. Finally, the moment method technique is briefly discussed in terms of its applicability to overmoded transition problems.

Manuscript received December 12, 1988; revised July 17, 1989.

W. A. Huting is with the Applied Physics Laboratory, Johns Hopkins University, Laurel, MD 20707.

K. J. Webb is with the Electrical Engineering Department, University of Maryland, College Park, MD 20742.

IEEE Log Number 8930797.

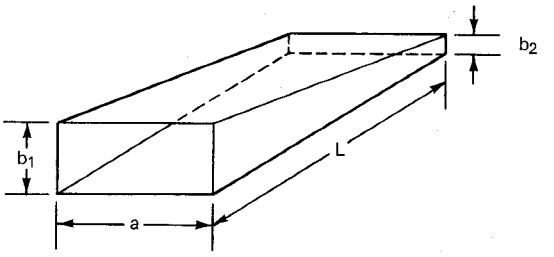

Fig. 1. Rectangular-to-rectangular waveguide transition.

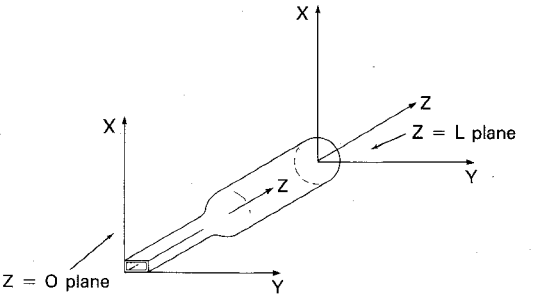

Fig. 2. Generalized waveguide transition geometry.

II. THE GENERALIZED TELEGRAPHIST'S EQUATION

One of the earliest theoretical treatments of nonuniform waveguides was given by Reiter [13], who utilized the well-known fact that uniform waveguide modal fields can be used as a complete orthogonal basis for physically realizable electromagnetic fields [14]. Extending this concept to waveguide transitions such as that shown in Fig. 2, he asserted that the transverse electromagnetic fields could be written as a sum of the transverse mode functions [13]:

$$\boldsymbol{E}_t(x, y, z) = \sum_{m=1}^{\infty} V_m(z)\boldsymbol{e}_m(x, y, z) \tag{1}$$

$$\boldsymbol{H}_t(x, y, z) = \sum_{m=1}^{\infty} I_m(z)\boldsymbol{h}_m(x, y, z) \tag{2}$$

where the parameters $V_m(z)$ and $I_m(z)$ are known respectively as the equivalent voltages and the equivalent currents. A discussion of the validity of (1) and (2) can be found in [9] and [16]. By inserting (1) and (2) into the transverse form of Maxwell's equations and applying the appropriate boundary conditions on the transition inner surface, one obtains the so-called generalized telegraphist's

equation [13], [15], [16]:

$$\frac{d}{dz}\begin{pmatrix} V_1 \\ V_2 \\ \vdots \\ I_1 \\ I_2 \\ \vdots \end{pmatrix} = \begin{pmatrix} T_{11} & T_{12} & \cdots & \gamma_1 Z_1 & 0 & \cdots \\ T_{21} & T_{22} & & 0 & \gamma_2 Z_2 & \\ \vdots & & & \vdots & & \\ -\gamma_1/Z_2 & 0 & \cdots & -T_{11} & -T_{21} & \cdots \\ 0 & -\gamma_2/Z_2 & & -T_{12} & -T_{22} & \\ \vdots & & & \vdots & & \end{pmatrix} \cdot \begin{pmatrix} V_1 \\ V_2 \\ \vdots \\ I_1 \\ I_2 \\ \vdots \end{pmatrix} \tag{3}$$

where

$$T_{ij} \equiv \int_S \int \boldsymbol{e}_j \cdot \frac{d\boldsymbol{e}_i}{dz} ds. \tag{4}$$

The variables γ_t in (3) are the complex propagation constants and the variables Z_t are the modal impedances. Solymar [17] decomposed the equivalent voltages and currents into forward- and backward-traveling waves and gave some approximate solutions to the resultant system of differential equations. Later, Saad *et al.* evaluated numerically the approximate expressions of Solymar for several transitions including the simple rectangular-to-rectangular transition [7] to be treated in this paper. Our approach deals with (3) directly. Let the two ends of the transition occur in the planes $z = 0$ and $z = \mathrm{L}$. What is sought is the hybrid matrix $(K(z))$ as defined by

$$\begin{pmatrix} V(z) \\ I(z) \end{pmatrix} = (K(z)) \begin{pmatrix} V(0) \\ I(0) \end{pmatrix}. \tag{5}$$

As noted in [10], the differential equation for $(K(z))$ is given by

$$\frac{d}{dz}(K) = (C) \cdot (K) \tag{6}$$

where (C) is the square matrix from (3). The initial condition used in the solution of (6) is

$$K(z = 0) = U \tag{7}$$

where U is the unit (or identity) matrix. In this paper, the matrix (K) is evaluated according to (6) and (7) and $(K(z = L))$ is subsequently used to calculate the generalized scattering matrix which characterizes the overall transition [18].

III. Solutions via a Moment Method Technique

The first step in our method of solution is to truncate the infinite system of ordinary differential equations given in (3). Let N denote the number of differential equations and let q denote the column of the (K) matrix for which a solution is sought. Equation (6) is written symbolically as

$$\frac{d}{dz} K_{mq} = \sum_{n=1}^{N} C_{mn} K_{nq} \tag{8}$$

with the boundary condition

$$K_{mq}(z = 0) = \delta_{mq} \tag{9}$$

where δ_{mq} is the Kronecker delta function. One physical interpretation for (8) and (9) is seen by comparison with (3). If the equivalent voltage or current occupying the qth position in the column vector in (3) is set equal to 1 at $z = 0$ and all other equivalent voltages and currents are set equal to zero at that position, then (3) is identical to (8) and (9), and solution of (8) and (9) simply gives the equivalent voltages and currents along the length of the transition under these conditions.

We now approximate each element K_{mq} as the sum of E expansion functions:

$$K_{mq}(z) = \sum_{l=1}^{E} \alpha_{lm} f_l(z). \tag{10}$$

In the discussion that follows, it will be assumed that $f_1(z = 0) = 1$, and that all the other expansion functions vanish at $z = 0$. Thus, the boundary condition represented by (9) becomes

$$\alpha_{1m} = \delta_{mq}. \tag{11}$$

As a first step in obtaining a solution for the remaining coefficients α_{lm}, we consider of set of $(E-1)$ weighting functions w_k. An inner product is defined by

$$\langle g, h \rangle = \int_0^L g(z) h(z)\, dz. \tag{12}$$

Combining (8) and (10) and taking the appropriate inner products, one obtains

$$\sum_{l=1}^{E} \left\langle w_k, \frac{df_l}{dz} \right\rangle \alpha_{lm} = \sum_{l=1}^{E} \sum_{n=1}^{N} \langle w_k, C_{mn} f_l \rangle \alpha_{ln}. \tag{13}$$

Rearranging (13) and making use of (11), one finds

$$\sum_{n=1}^{N} \sum_{l=2}^{E} \left(\left\langle w_k, \frac{df_l}{dz} \right\rangle \delta_{mn} - \langle w_k, C_{mn} f_l \rangle \right) \alpha_{ln} = -\left\langle w_k, \frac{df_1}{dz} \right\rangle \delta_{mq} + \langle w_k, C_{mq} f_1 \rangle. \tag{14}$$

Equation (14) may be written in matrix form as

$$(B) \cdot (\hat{\alpha}) = (c). \tag{15}$$

The elements of (B) are given by

$$b((m-1)(E-1)+k, (n-1)(E-1)+l-1) = \left\langle w_k, \frac{df_l}{dz} \right\rangle \delta_{mn} - \langle w_k, C_{mn} f_l \rangle \tag{16}$$

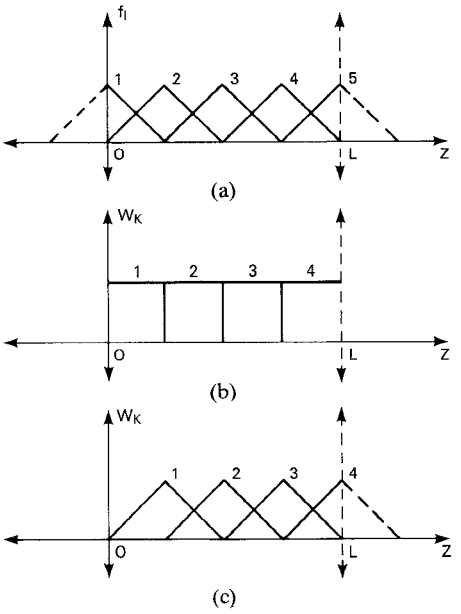

Fig. 3. Expansion and weighting functions for $E=5$. (a) Triangle expansion functions. (b) Pulse weighting functions. (c) Weighting functions for Galerkin's method.

with

$$1 \le m, n \le N$$
$$1 \le k \le E-1$$
$$2 \le l \le E.$$

Here $b(i, j)$ refers to the element occupying the ith row and jth column of (B). (B) is a square matrix with dimension $N(E-1)$. The elements of the column vectors $(\hat{\alpha})$ and (c) are given by

$$\hat{\alpha}((n-1)(E-1)+l-1) = \alpha_{ln} \tag{17}$$

$$c((m-1)(E-1)+k) = -\left(\left\langle w_k, \frac{df_1}{dz}\right\rangle \delta_{mq} + \langle w_k, C_{mq} f_1\rangle\right). \tag{18}$$

It should be noted that the matrix (B) is in no way dependent on which column of the (K) matrix is being evaluated.

In this paper, we use one set of expansion functions and two sets of weighting functions. The set of expansion functions consists of the subsectional triangles

$$f_l = \begin{cases} 1-(E-1)\left|\dfrac{z-z_l}{L}\right|, & \left|\dfrac{z-z_l}{L}\right| < \dfrac{1}{E-1} \\ 0 & \left|\dfrac{z-z_l}{L}\right| > \dfrac{1}{E-1} \end{cases}, \tag{19}$$

where

$$z_l = (i-1)\frac{L}{E-1}, \qquad i = 1,2,3,\cdots,E. \tag{20}$$

A graph of these triangle functions is given in Fig. 3(a). For weighting functions, one may choose a set of pulses

$$w_k = \begin{cases} 1, & z_k < z < z_{k+1} \\ 0, & \text{otherwise.} \end{cases} \tag{21}$$

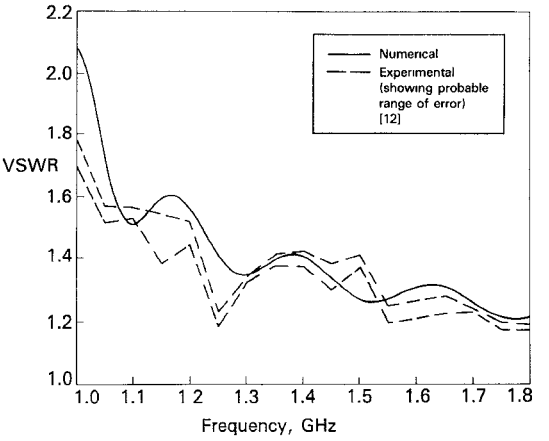

Fig. 4. Theoretical versus experimental *VSWR* for linear transition. The theoretical curve was generated considering only the TE10 mode. The same results were obtained using a Runge–Kutta technique, an iterative integration technique, and Galerkin's method with triangle expansion functions.

These pulses are shown in Fig. 3(b). There is one more expansion function than there are weighting functions. The "extra" expansion function, however, is $f_1(z)$, which has a known coefficient, determining (c). In this paper, the inner products which make up (B) are evaluated numerically using the midpoint rule [19] with 20 integration points per triangle base.

As an alternative to (21), one may use Galerkin's method, as illustrated in Fig. 3(c), where

$$w_k = f_{k+1}. \tag{22}$$

For this choice, the set of weighting functions is the same as the set of expansion functions (not counting the expansion function f_1, which has a known coefficient). Use of (19) and (22) is also termed a finite element method [20].

IV. Numerical Results

In this section, a simple linear single-mode transition between standard WR-650 waveguide and a waveguide with the same width but a smaller height is analyzed. The dimensions of this device are (Fig. 1): $a=6.500$ in, $b_1=3.250$ in, $b_2=0.400$ in, $L=19.392$ in. There are three reasons for choosing this transition as a test case. First of all, closed-form expressions are easily derived for the elements of the matrix in (3). Second, dimensions and experimental results (for TE_{10} incidence on the large end of the transition between 1.0 and 1.8 GHz) are given by Young [12]. Finally, this transition was also analyzed by Saad *et al.* [7]. They solved the one-mode version of Solymar's differential equation [17] by two methods, namely numerical integration of Solymar's approximate expressions and use of the standard IBM routine DLBVP [23], and they found the two computed *VSWR*'s to be in agreement to within 5 percent [7]. For the one-mode case, we solved (8) using a Runge–Kutta technique. Our computed *VSWR*, which is shown in Fig. 4 along with Young's experimental data, appears to be extremely close to [7, fig. 3]. Theory and experiment are in good agreement except below 1.1 GHz, where in the experiment the small end of the transi-

tion appears to have been poorly matched. We also solved the one-mode problem two other ways. One method consisted of successively integrating (6) until (K) converged to a solution. For the first iteration, (K) was set equal to the identity matrix. According to [10], this method, when applied to circular-to-circular transitions, yields the same results as discretizing the transition boundary and applying mode matching and uses a comparable amount of computer time. We found that by employing the midpoint rule [19] with 100 integration points, the *VSWR* curve approached that of Fig. 4 after 50 iterations. Finally, Galerkin's method was used with triangle expansion functions and $E = 31$. Condition numbers for (B) were computed by multiplying the one-norm of (B) by the one-norm of the computed inverse of (B). The reasons for computing this parameter are that a matrix with a high condition number tends to amplify errors due to factors such as roundoff. Condition numbers close to 1 are desirable [21]. Although the condition numbers were high (typically 4×10^5) the results for the *VSWR* and the (2×2) scattering matrix were identical to those computed using the Runge–Kutta technique. The reciprocity relation $S_{12} = S_{21}$ was extremely well satisfied by the moment method and the Runge–Kutta routines, but it was not well satisfied by the integration technique. The amounts of computer time used on the Hitachi NAS 9160 were seven seconds for the Runge–Kutta technique, six minutes for the integration technique, and six minutes for the Galerkin method program. The moment method routines described in this section all employed double precision (64 bit) arithmetic, while the one-mode Runge–Kutta and integration routines employed single precision arithmetic. None of the routines were optimized with respect to run time or storage.

When the evanescent TE_{11} and TM_{11} modes are included in (8), numerical instabilities occur in both the Runge–Kutta routine and the iterative integration technique. For the linear transition, a double precision version of the Runge–Kutta routine failed to converge even though the number of points was varied between 11 and 501. Similarly, a double precision version of the integration technique program also failed to converge. The method of moments was also used, taking the TE_{10}, TE_{11}, and TM_{11} modes into account. Fig. 5 shows the calculated *VSWR* for $E = 6,7,8,9,10$ using triangle expansion functions and Galerkin's method. For $E = 6$, condition numbers ranged from 2×10^8 to 2×10^9, while for $E = 10$, condition numbers were in the range 2×10^8 to 3×10^9. The computed *VSWR* seemed to agree with the experimental results on average with greater oscillations as E was increased. An alternative method of solution is to divide the transition into several sections of equal length, to analyze each section with $E = 6$, to cascade the several sections, and to compute the overall scattering matrix. Cascading simply involves multiplication of the (K) matrices representing each section. Fig. 6 shows the results when the transition was divided into one through six sections, again using Galerkin's method. For six sections, most of the condition numbers were in the range 3×10^7 to 1×10^8, and the

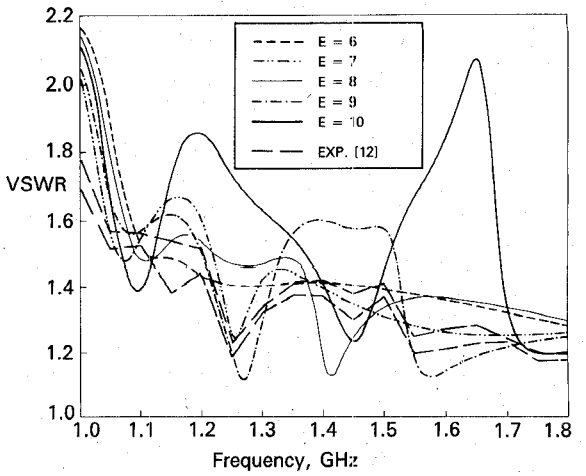

Fig. 5. Calculated *VSWR* using triangle expansion functions and Galerkin's method. The TE10, TE11, and TM11 modes were considered and the number of triangles E was varied.

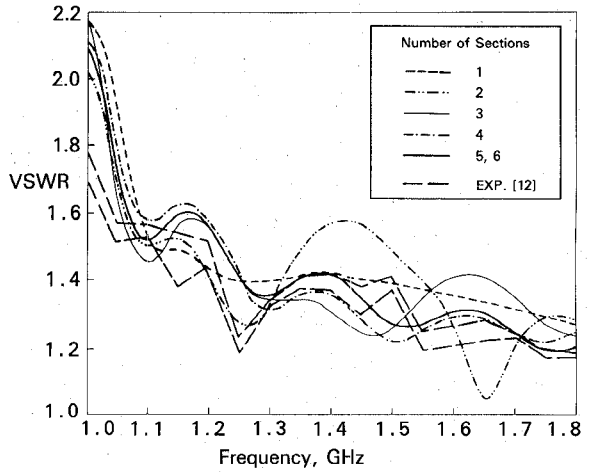

Fig. 6. Calculated *VSWR* using triangle expansion functions and Galerkin's method and considering the TE10, TE11, and TM11 modes. The transition was divided into several sections, each of which was analyzed with $E = 6$.

computed *VSWR* converged to a solution close to the single-mode solution described above. Also, the solutions for five and six sections were indistinguishable, indicating convergence. Finally, as a simple check on the validity of the Galerkin method program, a straight uniform waveguide was analyzed for $E = 6$ and for six cascaded sections. The computed (6×6) scattering matrices were close to the expected results, and condition numbers for (B) were, typically, about 10^7.

Another check on the validity of the Galerkin method program may be performed as follows. First, one writes the generalized scattering matrix in submatrix form:

$$\begin{pmatrix} b^1 \\ b^2 \end{pmatrix} = \begin{pmatrix} S^{11} & S^{12} \\ S^{21} & S^{22} \end{pmatrix} \begin{pmatrix} a^1 \\ a^2 \end{pmatrix} \tag{23}$$

where port 1 occurs in the $z = 0$ plane and port 2 occurs in the $z = L$ plane. The mode coefficients a^i and b^i are

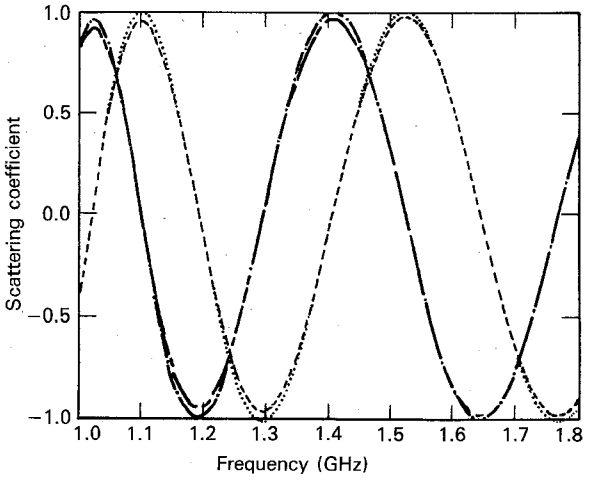

Fig. 7. Scattering parameters from (23) computed using Galerkin's method with $E=6$ and six cascaded section. Real (S_{11}^{12})—dot. Real (S_{11}^{21})—dash. Imag (S_{11}^{12})—chaindot. Imag (S_{11}^{21})—chaindash.

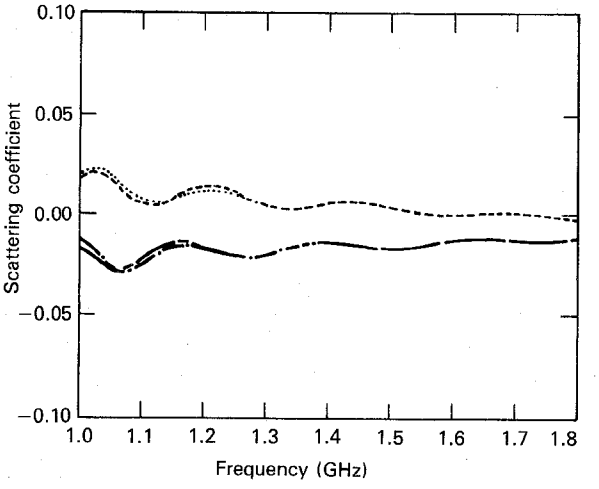

Fig. 8. Scattering parameters from (23) computed using Galerkin's method with $E=6$ and six cascaded sections. Real (S_{12}^{11})—dot. Real (S_{21}^{11})—dash. Imag (S_{12}^{11})—chaindot. Image (S_{21}^{11})—chaindash.

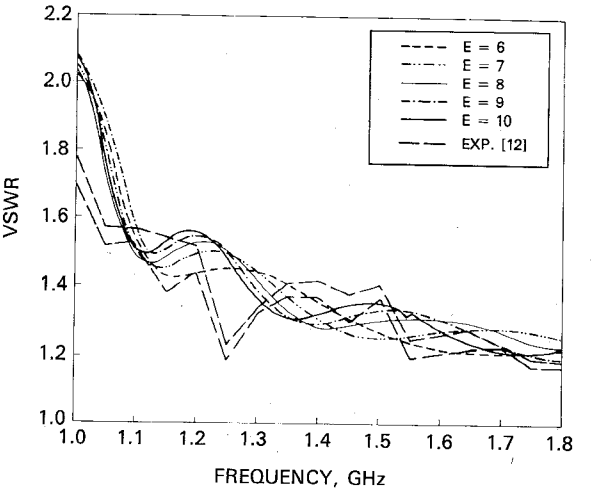

Fig. 9. Calculated *VSWR* using triangle expansion functions and pulse weighting functions and considering the TE10, TE11, and TM11 modes. The number of triangles E was varied.

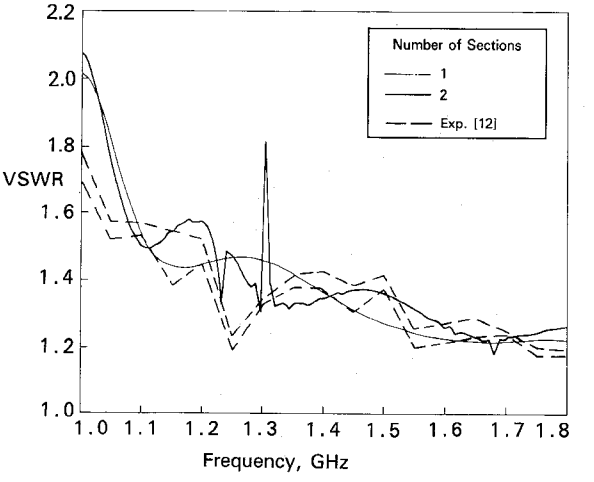

Fig. 10. Calculated *VSWR* using triangle expansion functions and pulse weighting functions and considering the TE10, TE11, and TM11 modes. The transition was divided into several sections, each of which was analyzed with $E=6$.

explicitly written as

$$a^i = \begin{pmatrix} a^i_{\mathrm{TE01}} \\ a^i_{\mathrm{TE11}} \\ a^i_{\mathrm{TM11}} \end{pmatrix} \qquad b^i = \begin{pmatrix} b^i_{\mathrm{TE01}} \\ b^i_{\mathrm{TE11}} \\ b^i_{\mathrm{TM11}} \end{pmatrix} \tag{24}$$

where i denotes the port (1 or 2). The submatrices S^{11}, S^{12}, S^{21}, and S^{22} have been truncated to 3×3. From the Lorentz reciprocity theorem, using normalized modes, one may derive $S_{ij}^{11}=S_{ji}^{11}$, $S_{ij}^{21}=S_{ji}^{12}$, and $S_{ij}^{22}=S_{ji}^{22}$. These requirements are poorly satisfied when Galerkin's method is used with $E=6$ and one section but well satisfied for $E=6$ and six cascaded sections. Figs. 7 and 8 show several of the computed scattering parameters as a function of frequency for this later case.

One possible explanation for the numerical problems which occur in the three-mode case may lie in the fact that (C) has higher condition numbers in the three-mode case $(4\times10^5$ to $3\times10^6)$ than in the one-mode case (typically 4×10^5). Both the Runge–Kutta technique and the iterative integration technique involve repeated use of (C). In comparison, the Galerkin method program involves a matrix (B) which has a condition number somewhat higher than that of (C), but it uses that matrix (B) only once, in the solution of (15).

Fig. 9 shows the calculated *VSWR* for $E=6,7,8,9,10$ using the method of moments with triangle expansion and pulse weighting functions. Computed condition numbers ranged between 2×10^8 and 3×10^8 for $E=6$ and between 10^{12} and 10^{13} for $E=10$. Dividing the transition into several cascaded sections was also attempted and the results are shown in Fig. 10. The condition numbers ranged between 10^9 and 4×10^{11} for two sections and $E=6$. In no case were the reciprocity relations well satisfied for the pulse weighting function method. For E larger than 10, or for more than two cascaded sections, the results became unstable.

To summarize, of the techniques examined here, only Galerkin's method (with cascading) converges to a satis-

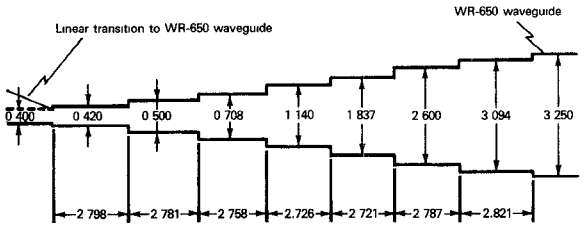

Fig. 11. Young's experimental setup with dimensions in inches.

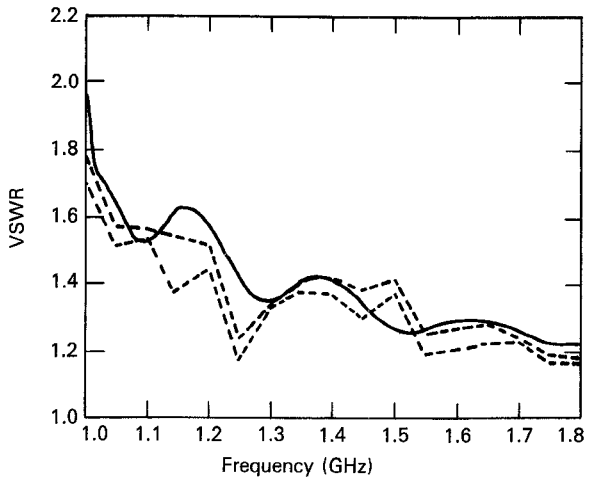

Fig. 12. Calculated *VSWR* using Galerkin's method, considering the TE10, TE11, TM11, and TM11 modes, dividing the transition into six sections, each of which was analyzed with $E = 6$, and taking into account the characteristics of the step transformer.

factory solution with the inclusion of evanescent modes. The *VSWR* for this example transition is very close to the *VSWR* computed using only one mode. Agreement between these curves and Young's experimental data [12] is good, except below 1.1 GHz. This agreement may be improved as follows. Up to now, a perfect match has been assumed at the $z = L$ plane. In fact, the transition was mated with an eight-step transformer (Fig. 11). The characteristics of this transformer were analyzed using a mode-matching technique with three modes in each section (e.g., [22]). The scattering matrix of the transformer may be linked together with the scattering matrix of the linear transition to describe the behavior of the overall system. When this is done to the Galerkin method (three modes, six cascaded sections) procedure for the linear transition, the *VSWR* curve takes the form shown in Fig. 12. This curve shows very little change above 1.1 GHz. Below 1.1 GHz, however, agreement between theory and experiment is greatly improved.

V. Conclusion

A simple waveguide transition has been analyzed by generating a solution to the generalized telegraphist's equation via a moment method technique. Numerical stability and accuracy and consistency of the results are critically dependent on the choice of weighting and expansion functions. The best results for a simple rectangular-to-rectangular transition were obtained when Galerkin's method and triangle expansion functions were applied to several short sections which were then cascaded. Unlike the Runge–Kutta technique or the integration technique, the Galerkin's method procedure did not result in instabilities with the inclusion of evanescent modes. Our programs can, in fact, be extended to any number of modes, the only apparent limitations being the obvious ones of computer time and memory, and all three techniques are now being studied for possible applicability to the analysis of transitions between rectangular single-mode and circular overmoded waveguide such as the Marie transducer (e.g., [6], [7]) and the multiport transition described in [8].

References

[1] R. E. Collin, *Field Theory of Guided Waves*. New York: McGraw-Hill, 1960, pp. 195–198.
[2] *Bell Syst. Tech. J.*, Special issue on the WT4 Millimeter Waveguide System, vol 56, Dec. 1977.
[3] S. Iiguchi, "Mode conversion in the excitation of TE_{01} waves in a TE_{01} mode transducer (rectangular → sector portion → circular)," in *Proc. Symp. Millimeter Waves* (Polytechnic Institute of Brooklyn, New York), Mar. 1959, pp. 595–618.
[4] Y. M. Isayenko, "$H_{10} - H_{02} - H_{01}$ continuous transformer," in *Proc. 3rd Colloq. Microwave Commun.* (Budapest, Hungary), Apr. 1966, pp. 467–475.
[5] F. Sporleder, "Waveguide transition design of improved accuracy," *Arch. Elek. Übertragung.*, vol. 30, pp. 289–296, 1976.
[6] S. S. Saad, J. B. Davies, and O. J. Davies, "Analysis and design of a circular TE_{01} mode transducer," *IEE J. Microwaves, Opt., Acoust.*, vol. 1, pp. 58–62, Jan. 1977.
[7] S. S. Saad, J. B. Davies, and O. J. Davies, "Computer analysis of gradually tapered waveguide with arbitrary cross-sections," *IEEE Trans. Microwave Theory Tech.*, vol. MTT-25, pp. 437–440, May 1977.
[8] W. H. Zinger and J. A. Krill, "Multiport rectangular TE_{10} to circular TE_{01} mode transducer having pyramidal shaped transducing means," U.S. Patent 4,628,287, Dec. 9, 1986.
[9] H.-G. Unger, "Circular Waveguide taper of improved design," *Bell Syst. Tech. J.*, vol. 37, pp. 899–912, 1958.
[10] H. Flügel and E. Kühn, "Computer-aided analysis and design of circular waveguide tapers," *IEEE Trans. Microwave Theory Tech.*, vol. 36, pp. 332–336, Feb. 1988.
[11] R. F. Harrington, *Field Computation by Moment Methods*. New York: McGraw-Hill, 1968.
[12] L. Young, "Practical design of a wide-band quarter-wave transformer in waveguide," *Microwave J.*, vol. 6, pp. 76–79, Oct. 1963.
[13] G. Reiter, "Generalized telegraphist's equation for waveguides of varying cross-section," *Proc. Inst. Elec. Eng.*, vol. 106B, suppl. 13, pp. 54–57, Sept. 1959.
[14] J. D. Jackson, *Classical Electrodynamics*, 2nd ed. New York: Wiley, 1975.
[15] F. Sporleder and H.-G. Unger, *Waveguide Tapers, Transitions, and Couplers*, New York: Peter Peregrinus, 1979.
[16] W. A. Huting, "Rectangular to circular waveguide transitions for high power circular overmoded waveguides," TG-1375, The Johns Hopkins University Applied Physics Laboratory, Laurel, Md. 1989.
[17] L. Solymar, "Spurious mode generation in nonuniform waveguide," *IRE Trans. Microwave Theory Tech.*, vol. MTT-7, pp. 379–383, July 1959.
[18] R. Mittra and S. W. Lee, *Analytical Techniques in the Theory of Guided Waves*. New York: MacMillan, 1971, p. 208.
[19] P. J. Davis and P. Rabinowitz, *Numerical Integration*. Waltham, MA: Blaisdell, 1967, p. 15.
[20] E. B. Becker, G. F. Carey, and J. T. Oden, *Finite Elements: An Introduction*. Englewood Cliffs, N.J.: Prentice-Hall, 1981.
[21] G. E. Forsythe, M. A. Malcom, and C. B. Moler, *Computer Methods for Mathematic Computations*. Englewood Cliffs, NJ: Prentice Hall, 1977, pp. 41–47.
[22] L. Carin, K. J. Webb, and S. Weinreb, "Matched windows in circular waveguide," *IEEE Trans. Microwave Theory Tech.*, vol. 36, pp. 1359–1362, Sept. 1988.
[23] "Subroutines LBVP and DLBVP," in System/360 Scientific Subroutine Package, Version III, IBM Programmer's Manual No. 360A-CM-03X, IBM, 1968, pp. 350–360.

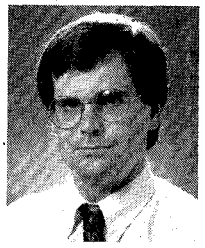

William A. Huting (S'80–M'84) was born in Ann Arbor, MI, on June 23, 1959. He received the B.S.E. degree in electrical engineering from Duke University in 1981, the M.S.E.E. degree from Georgia Tech in 1982, and the Ph.D. degree in electrical engineering from the University of Maryland in 1989.

Since 1984, he has been with the Applied Physics Laboratory, Johns Hopkins University, where he has principally been involved with investigations of circular overmoded waveguide and tapered waveguide transitions.

✠

Kevin J. Webb (S'80–M'84) was born in Stawell, Victoria, Australia, on July 7, 1956. He received the B.Eng. and M.Eng. degrees in communication and electronic engineering from the Royal Melbourne Institute of Technology, Australia, in 1978 and 1980, respectively, the M.S.E.E. degree from the University of California, Santa Barbara, in 1981, and the Ph.D. degree in electrical engineering from the University of Illinois, Urbana, in 1984.

Since 1984, he has been an Assistant Professor in the Electrical Engineering Department at the University of Maryland, College Park. His research interests include microwave and millimeter-wave integrated circuits, VLSI circuits, optoelectronics, numerical electromagnetics, and frequency selective surfaces.

Dr. Webb is a member of Tau Beta Pi, Eta Kappa Nu, and Phi Kappa Phi.